Communication

3D Printed Directive Beam-Steering Antenna Based on Gradient Index Flat Lens With an Integrated Polarizer for Dual Circular Polarization at W-Band

J. Melendro-Jimenez, P. Sanchez-Olivares, A. Tamayo-Dominguez, X. Sun, and J. M. Fernandez-Gonzalez

***Abstract*— In this communication, the design of a circularly polarized (CP) perforated gradient index (GRIN) flat lens antenna with directive beam-steering properties is presented for millimeter-wave applications at W-band (75–95 GHz). The dielectric lens, fed by an open-ended square waveguide (SWG) located in the lens focal plane, enhances the radiation in a particular direction, generating a high-directivity beam with planar wavefront. The integration of a dielectric polarizer with the lens allows the conversion from a linearly polarized (LP) incident wave to a CP-emitted wave over the whole bandwidth. Horizontally and vertically polarized waves, achieved by the excitation of the fundamental SWG TE_{01} and TE_{10} modes are transformed into left-hand CP and right-hand CP waves, respectively. A ±30° scan range in both azimuth and elevation planes is demonstrated for the whole frequency range, attained by displacing the feed along the focal plane of the lens. Lens and polarizer are manufactured as a single piece by stereolithography (SLA) 3-D printing technology with Form 3 Formlabs 3-D-printer. Measured results show maximum measured directivity values that range from 23.5 to 23.8 dB, a remarkable circular polarization purity as a wide axial ratio bandwidth of 20.58% (<3 dB), from 77.5 to 95 GHz, is achieved for the principal beam steers and an aperture efficiency for broadside beam direction between 90.32% and 57.34% in the frequency band of interest.**

***Index Terms*— Beam steering, circular polarization, lens antennas, reconfigurable antennas.**

I. Introduction

Recent advances in the most cutting-edge engineering disciplines, such as tracking applications or collision avoidance systems, come along with the necessity of new millimeter-wave technologies and more compact antenna designs [1], [2]. Millimeter-waveband applications require highly directive antenna beam patterns to compensate the large attenuation losses. Some antenna realizations in this frequency range efficiently enhance the gain, yet at the expense of incorporating large feeding networks or entailing complex manufacturing techniques [3], [4]. Another approach for high-gain antennas that provides a much more compact and effective solution is dielectric lens antennas, which are usually combined with low-gain feed systems [5], [6], [7], [8]. The lens enhance the directivity of the low-gain feed by collimating the source rays into a single direction, generating a plane or quasi-plane wave. In some designs, when combined with a feed with beam reconfiguration capability, the lens compensates for the high scan losses, enhancing its directivity within the matched scan range [9], [10], [11]. The conventional alternative to these is phased array antennas. However, a standard phased array needs active elements to achieve beam steering, which are hardly available in W-band. Other alternatives are systems based on radio-frequency microelectromechanical (RF-MEM) devices or liquid crystal reflectarrays [12]. However, these technologies are on ongoing research and usually exhibit high losses.

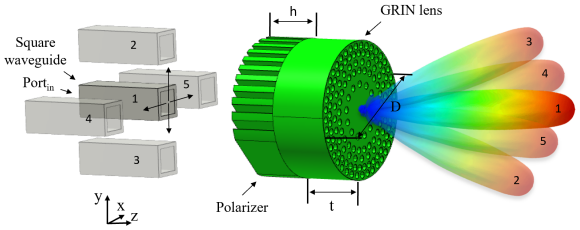

Fig. 1. Geometry of the proposed dual-CP GRIN flat lens with integrated polarizer fed by a SWG.

Although most of the previous works effectively cover the gain and form-factor requirements for millimeter-wave applications, almost all of them are linearly polarized (LP) designs. The traditional approach to design circularly polarized (CP) lens antennas is by adding a CP feed. In [13] a circular waveguide terminated in a small horn is integrated with a dielectric septum polarizer to feed a dielectric lens. Besides, in [14] a dielectric septum polarizer integrated in a circular waveguide is combined with a dielectric rod antenna to feed dielectric spheres lenses. These solutions have some drawbacks, such as the increase in the complexity of the design. A dielectric septum is a highly tolerance-sensible approach, as the slightest thickness variation implies noticeable magnitude and phase deviations [15]. Although there have been some proposals for large tolerance optimization strategies [16], no effectual solution exists yet for upper millimeter wave bands. Thus, to address the above-mentioned problems and requirements at once, an LP feed with a low-cost CP lens is the fitting solution. Moreover, dual circular polarization is an essential requirement in applications such as satellite communications [17] and it is being increasingly demanded in new millimeter-wave wireless communications, as it enables polarization division multiplexing (PDM) [18] and in-band full duplex (IBFD) [19], achieving an enhanced spectral efficiency, thus increasing the throughput of wireless communication systems.

In this communication, a beam-steering dual CP flat lens antenna designed to operate in the lower part of the W-band is presented. The antenna consists of a square waveguide (SWG) and a perforated gradient index (GRIN) flat lens with an integrated polarizer (Fig. 1). The polarizer consists of parallel dielectric slabs that convert incident LP waves into CP ones [20]. GRIN lens and polarizer (CP lens) are optimized to maximize the directivity of the design by means of a maximization of the aperture efficiency. The SWG illuminates the lens with a horizontally or vertically polarized wave which is converted into a left-handed CP (LHCP) or right-handed CP (RHCP) wave, respectively. Beam tilting capability is accomplished

Manuscript received 6 May 2022; revised 29 September 2022; accepted 14 October 2022. Date of publication 31 October 2022; date of current version 19 January 2023. This work was supported by the Spanish Government, Ministry of Economy, National Program of Research, Development and Innovation under the Project New Array Antenna Technologies and Digital Processing for the Future Integrated Terrestrial and Space-Based Millimeter Wave Radio Systems—UPM-InTerSpaCE under Grant PID2020-112545RB-C51. *(Corresponding author: P. Sanchez-Olivares.)*

The authors are with the Information Processing and Telecommunications Center (IPTC), ETSI Telecomunicación, Universidad Politécnica de Madrid, 28040 Madrid, Spain (e-mail: javier.melendro.jimenez@upm.es; pablo.sanchezo@upm.es; a.tamayo@upm.es; x.sun@upm.es; josemanuel.fernandez.gonzalez@upm.es).

Color versions of one or more figures in this communication are available at https://doi.org/10.1109/TAP.2022.3217177.

Digital Object Identifier 10.1109/TAP.2022.3217177

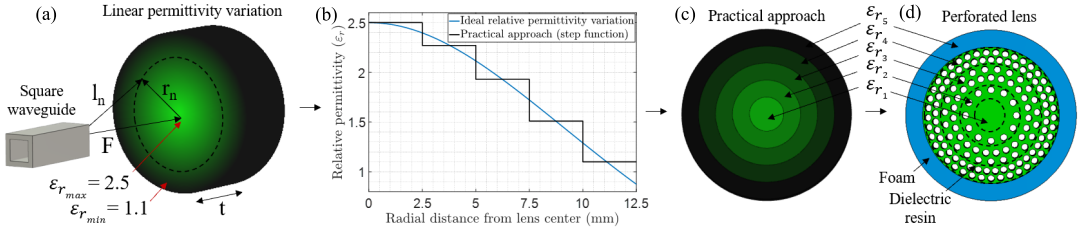

Fig. 2. Relative permittivity distribution as a function of radius. (a) Ideal case: linear radial decrease of dielectric permittivity. (b) Ideal case versus practical approach. (c) Practical approach: five-layer lens. (d) Perforated lens.

by displacing the SWG in x- and y-axis along the focal plane of the lens, achieving a $\pm 30°$ scanning range in both azimuth and elevation planes. The lens and the integrated polarizer are manufactured as a single piece by stereolithography (SLA) 3-D printing technology, which is a straightforward and low-cost manufacturing approach. Gray resin material and the Form 3 Formlabs 3-D-printer have been utilized for the manufacture. Thus, the novelty of this work resides in the fact that the presented CP lens gathers in a monolithic and compact low-budget 3-D-printable design a high-gain beam-steering and dual CP antenna to be used in many W-band applications.

II. CP Lens Antenna Design

This section will address the design procedure of the CP lens antenna, which consists of the integration of a GRIN flat lens with a dielectric cylindrical polarizer (Fig. 1). The GRIN lens is a 20-mm diameter (D) and 8.5-mm thick (t) flat lens consisting of five radial layers of gradual decreasing relative permittivity (varying values from 2.5 to 1.1), that operates within the 75–95 GHz band. The radial layered degression of relative permittivity is attained by precisely distributing air holes across the dielectric lens. Then, the effective volume of each layer can be precisely varied, thus adjusting the required effective permittivity. The dielectric polarizer consists of 7 mm height (h) parallel dielectric slabs that convert LP waves into CP ones. The feed element for the designed CP lens is an SWG of 2.15 x 2.15 mm and an 8.15 dBi peak directivity at 85 GHz. The diameter of the lens value has been fixed looking for a compromise between a reduced form-factor of the antenna and a proper directivity enhancement. For this application, the TE_{10} mode is excited to generate RHCP, whereas the TE_{01} mode must be excited for LHCP. The SWG is aligned on the focal plane of the lens, so the radiation coming from it can be collimated into a single direction, generating a planar wavefront. When the feed phase center is placed in the focal point, a highly directive broadside beam is radiated by the GRIN lens. However, by applying vertical and horizontal displacements on the SWG position along the focal plane, the main beam radiated by the lens can be tilted within a $\pm 30°$ scanning range at the expense of a loss of directivity for both azimuth and elevation planes. Lens and polarizer are integrated and manufactured as a single piece by SLA-3-D printing.

A. Theoretical Study of Permittivity Distribution

The GRIN flat lens is excited by a spherical wavefront emitted by the SWG, located in the far-field region of the lens. The distance from the focal point to each point of the surface of the lens varies, which causes the different rays that go through the lens are not in phase. For the lens to generate a planar wavefront, every ray traveling through free space and past the lens should suffer the same phase delay. This aspect is discussed in [21], where it is shown that the phase variation between two different paths can be compensated by the following:

$$k_0 F + k_1 t = k_0 l_n + k_n t. \tag{1}$$

As seen in Fig. 2(a), F is the focal length, l_n is the distance from the focal point to a generic radial layer "n" of the lens, which can be expressed as $(F^2 + r_n^2)^{1/2}$, being r_n the radius of that generic layer. The parameter t is the already addressed lens thickness and k_n corresponds to the wavenumber of the generic layer. Therefore, the formula implies that the phase delay of a ray that travels through free space and past the central layer of the lens must be the same as the phase delay of a ray that travels through free space and past a generic lens layer. The wavenumber is dependent on the electric permittivity as $k_n = 2\pi(\sqrt{\varepsilon}_{r_n}/\lambda_0)$, so the dielectric constant for each layer can be precisely adjusted to reach the desired phase compensation for planar wave emission.

Having prior knowledge of the permittivity values of the central and edge layer of the lens, which are 2.5 for unaltered Gray resin and 1.1 for Foam, respectively, parameters $F = 10.5$ mm and $t = 8.5$ mm were fixed to optimize the phase compensation between both layers using (1). Then, relative permittivity values required for phase compensation can be depicted as a function of the radial distance also using (1). This relative permittivity profile is illustrated in Fig. 2(b), where it can be observed that for an ideal phase compensation, the relative permittivity of the dielectric GRIN lens should linearly decrease from the center of the lens to its edges. However, a feasible approach is to approximate the depicted ideal profile to a step function, where each step corresponds to a homogeneous layer with a given relative permittivity value. Therefore, a five radial layer GRIN lens, shown in Fig. 2(c), is proposed for phase compensation. The selected relative permittivity values are 2.5, 2.27, 1.91, 1.52, and 1.1, from the central to the edge layer, respectively. However, this realization is complex due to the difficulty of acquiring commercial materials with this exact permittivity values. Thus, a single material perforated GRIN lens is proposed and described in Section II-C.

B. Study of Perforations and Final Lens

The relative permittivity of a dielectric material can be modified by reducing or increasing its effective volume. Following this premise, a dielectric lens of uniform relative permittivity constant of 2.5 is perforated to achieve a radial layered reduction of its effective volume and subsequently of its effective permittivity. By precisely adjusting the effective volume of each radial layer, the aforementioned required relative permittivity values can be obtained.

For this purpose, a triangular air hole lattice configuration is performed [22]. In this topology, if the perforation's diameter (d) and the separation between perforations (s) are small compared to the operational wavelength, a uniform effective permittivity value can be obtained for the whole layer. With (see [22, eq. (2)]), the effective dielectric permittivity (ε_{eff}) can be computed as a function of the filling factor (α), which as shown in (see [22, eq. (4)]), is dependent on the relation d/s. Parameter d is fixed to 1 mm, imposed by manufacturing limitations, so to obtain different values for α, s should be varied. Thus, by precisely adjusting the distance between perforations in each layer, the required filling factor for the sought relative permittivity for each layer can be obtained. The perforated GRIN lens is shown in Fig. 2(d). The obtained relative permittivity values for layers one to five are 2.5, 2.27, 1.91, 1.68, and 1.1, respectively. The following step, described in Section II-D, is the design of the polarizer and its integration with the perforated GRIN lens.

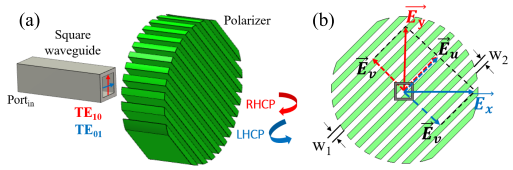

Fig. 3. Polarizer. (a) Dual-LP to dual-CP conversion. (b) Front view.

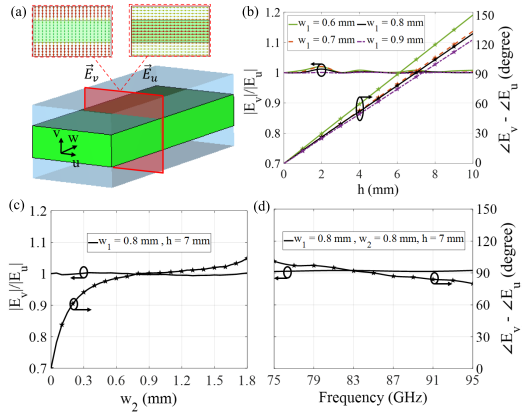

Fig. 4. Polarizer parametric analysis. (a) Unit cell. (b) Relation between orthogonal electric field components that propagate through the polarizer as a function of w_1 and h. (c) Function of w_2 and (d) in-band behavior for optimal configuration ($w_1 = 0.8$ mm, $w_2 = 0.8$ mm, and $h = 7$ mm).

C. Polarizing Structure

As it has been discussed, a cylindrical polarizer, consisting of parallel equally spaced dielectric slabs, is attached to the GRIN lens to convert LP waves into CP ones. The polarizer is tilted 45°, so if an LP wave is decomposed in its two orthogonal components, each of them is affected differently by the dielectric slabs, as the effective propagation constant of each component is different. Thus, by adjusting the polarizer dimensions, it is possible to generate a 90° phase shift between them, achieving LP to CP conversion. RHCP or LHCP can be obtained if exciting the polarizer with vertical or horizontal polarizations, respectively [see Fig. 3(a)]. The polarizer could be attached before or after the GRIN lens, as its polarization conversion capabilities remain unaltered. However, it was positioned between the SWG and the GRIN lens in order to reduce the volume of the entire antenna system.

The dual-LP to dual-CP conversion process is graphically pictured in Fig. 3(b). When the TE$_{10}$ mode is excited in the feeding SWG, a vertically polarized electric field ($\vec{E}_y$) is radiated. The $\vec{E}_y$ field is decomposed in a +45° tilted component ($\vec{E}_u$), parallel to the dielectric slabs of the polarizer, and a –45° tilted component ($\vec{E}_v$), orthogonal to the dielectric slabs. The polarizer will delay $\vec{E}_u$ with respect to $\vec{E}_v$, generating a 90° phase shift between them, thus obtaining RHCP from an impinging vertically polarized wave. Likewise, the $\vec{E}_x$ radiated field generated by the excitation of the TE$_{01}$ mode in the SWG is also decomposed in a +45° tilted component ($\vec{E}_v$) and a –45° tilted component ($\vec{E}_u$). $\vec{E}_u$ is delayed 90° with respect to $\vec{E}_v$, thus obtaining LHCP from an impinging horizontally polarized wave.

The circular polarization purity is optimized by means of adjusting the dimensions of the dielectric slabs. Thus, to design the polarizer and achieve linear to circular polarization conversion, a polarizer single unit cell has been analyzed [see Fig. 4(a)]. The length and the width of the slabs are h and w_1, respectively, and the separation between them is w_2. Therefore, the single unit cell consists of a w_1 thick and h length dielectric slab and two $w_2/2$ thick and h length air slabs. When an electric field vector parallelly polarized with respect to the dielectric slab ($\vec{E}_u$) propagates along the unitary cell, the electric field concentrates in the dielectric slab, whereas when an electric field vector orthogonally polarized with respect to the dielectric slab ($\vec{E}_v$) propagates along the unitary cell, the electric field concentrates in the air slabs. The electric field is distributed differently in each case, so two different propagation constants can be defined, γ_u and γ_v, with different phase constants, β_u and β_v. It can be observed in Fig. 4(a) that $\vec{E}_u$ concentrates in the dielectric, whereas $\vec{E}_v$ concentrates in the air slabs, thus $\beta_v < \beta_u$. So, as $\vec{E}_v$ and $\vec{E}_u$ propagate along the polarizer, the phase difference between them increases. To obtain circular polarization, a 90° phase shift and an amplitude relation of 1 between both components are sought. So, the phase difference and the amplitude relation between both electric field orthogonal components that propagate along the structure of Fig. 4(a) have been analyzed by means of a parametric study of w_1 and h, shown in Fig. 4(b). For this case, the total thickness of the cell is fixed to 1.6 mm (i.e., $w_1 + w_2 = 1.6$ mm). It is found that for $w_1 = 0.8$ mm, $h = 7$ mm and, therefore, $w_2 = 0.8$ mm, that condition is achieved. The phase difference and amplitude relation are analyzed for $w_1 = 0.8$ mm and $h = 7$ mm as a function of w_2 in Fig. 4(c) ($w_1 + w_2 = 1.6$ mm is not considered anymore), showing that the separation between dielectric slabs is not a determinant parameter when designing the polarizer, as a 90°±10° difference between electric field orthogonal components is achieved for values between $w_2 = 0.4$ mm and $w_2 = 1.8$ mm and an amplitude relation of 1 is obtained for the whole w_2 range. Finally, the optimal $w_1 = 0.8$ mm, $w_2 = 0.8$ mm, and $h = 7$ mm configuration is analyzed in the frequency band of interest in the detail of Fig. 4(d), presenting a reasonably good stability in the whole frequency band. The minimum and maximum phase difference between both components are 80° and 101°, respectively, whereas the amplitude relations are 1.004 and 1.007, respectively, almost a negligible drift from the expected value, 1. For the central frequency, perfect circular polarization is achieved, as 90° and 1.006 are obtained for the phase difference and amplitude relation between electric field orthogonal components.

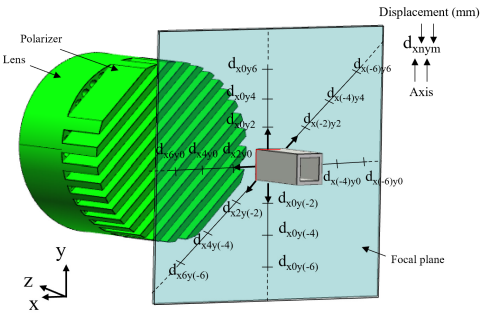

Fig. 5. Coordinate system for SWG displacements along lens focal plane.

III. Simulated Results

The proposed antenna has been simulated in *CST Microwave Studio*. Regarding the focal distance, it was optimized to a final value of $F = 11$ mm to enhance the plane wave conversion capability of the lens. Fig. 5 shows the defined coordinate system to which all antenna radiation result figures will refer. The SWG is displaced in discrete steps of 2 mm along x- and y-axis to precisely analyze the beam tilting characteristic. SWG displacements are labeled as d$_{xnym}$, where x and y refer to the axis along which the SWG is displaced, whereas n and m refer to the value of the displacement in millimeters along those axes, respectively.

The scanning performance of the design is evaluated for both polarizations, RHCP and LHCP, along the $\varphi = 0°$, 45°, and 90° cuts (Fig. 6). In-band axial ratio is also analyzed for each beam to evaluate the CP purity. Regarding the $\varphi = 0°$ and 90° cuts, it should be noted that due to the symmetry of the design, y-axis SWG

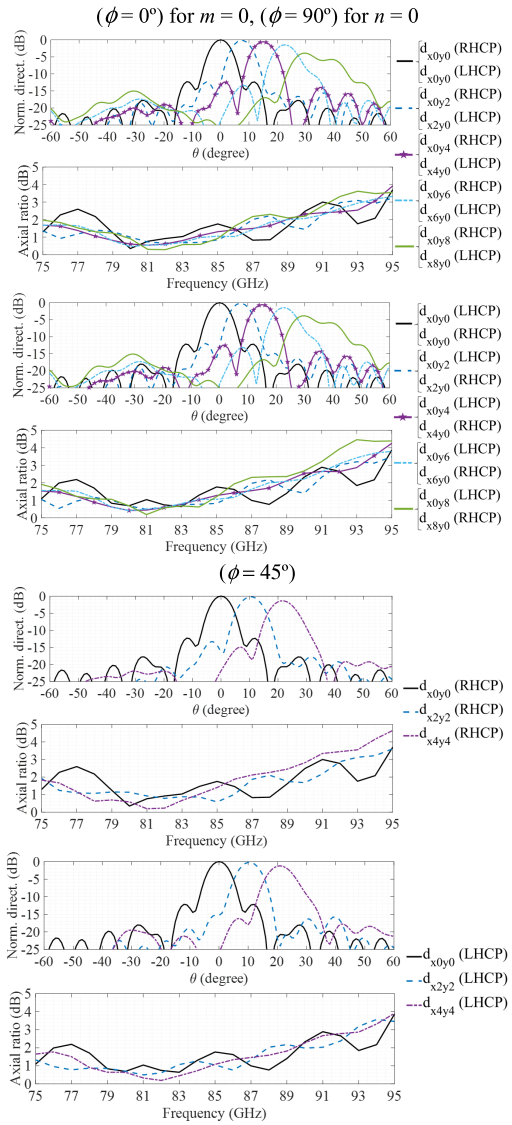

Fig. 6. Simulated beam reconfigurability at 85 GHz and in-band axial ratio.

displacements with TE_{10} or TE_{01} excitation are equivalent to x-axis SWG displacements with TE_{01} or TE_{10} excitation, respectively. When the SWG is displaced, the beam is steered off boresight up to 30°. As the GRIN lens is rotationally symmetric in XY plane, a scan range of ±30° is achieved for both azimuth and elevation planes. Scan losses vary from 0.2 dB for d_{x0y2} and d_{x2y0} to a maximum of 3.8 dB for the extreme steers, d_{x0y8} and d_{x8y0}, which is similar to the scan losses exhibited by other dielectric lenses, such as [5] and [6]. Main beam directions for d_{x0y0}, d_{x0y2}/d_{x2y0}, d_{x0y4}/d_{x4y0}, d_{x0y6}/d_{x6y0} and d_{x0y8}/d_{x8y0} are $\varphi = 0°/90°$ and $\theta = 0°$, 8°, 15°, 22.5° and 30°, respectively. Regarding the circular polarization purity, the axial ratio for both polarizations has been optimized for the beams obtained when the SWG is displaced, so as the beam is steered off boresight, an improvement on the correspondent axial ratio curves is obtained. Defining a 3 dB axial ratio criteria, a 20.8% (75–92.5 GHz) band is obtained for dual-CP applications. It is interesting to note that the integration of the polarizer with the GRIN lens in a monolithic, compact CP lens adds a slight ripple to the AR curves. However, the polarizer acts as a matching layer, reducing the power reflections in the air-lens interface, thus reducing back radiation, side lobe level (SLL) and increasing the directivity, as well as enhancing the scanning capability of the antenna.

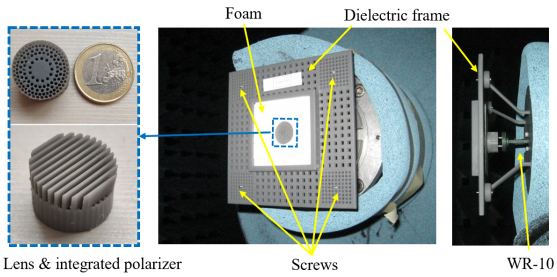

Fig. 7. Manufactured GRIN lens with integrated polarizer along with foam casing and dielectric gridded frame.

Regarding the $\varphi = 45°$ cut, d_{x0y0}, d_{x2y2}, and d_{x4y4} displacements are depicted for both RHCP and LHCP, along with the correspondent in-band axial ratio curves for each beam. Main beam directions for the three displacements are $\varphi = 45°$ and $\theta = 0°$, 10°, and 21°, respectively. Scan losses vary from 0.23 dB, for d_{x2y2}, to 1.39 dB, for d_{x4y4}. In-band axial ratio curves are below 3 dB for both polarizations and d_{x0y0}, d_{x2y2}, d_{x4y4} displacements, thus validating the LP to CP conversion for diagonal SWG displacements.

The dielectric polarizer has loss of about 2 dB. As a low loss alternative, it could be proposed to eliminate the polarizer and use an orthomode transducer to illuminate the GRIN lens with circular polarization. Nevertheless, the dielectric polarizer is a much simpler proposal from a technical and manufacturing point of view, a very important aspect when working at very high frequencies, as well as being considered low cost due to the use of 3-D printing technology. It is much less sensitive to manufacturing tolerances than W-band waveguide structures, which typically require considerably stringent resolution and tolerance requirements.

IV. Manufacturing and Measurements

The 3-D manufacturing process is illustrated in this section along with the measured results of the proposed antenna. The manufacturing is based on an SLA 3-D printing process [23]. This technique improves the overall performance of the 3-D printing process compared to other printing technologies, such as the fused deposition modeling (FDM) technique. SLA 3-D printing can produce objects with more than double the resolution of FDM printers [24]. However, the fact that FDM plastics exhibit lower dielectric losses [25] make this printing process a more suitable approach for applications in which antenna features sizes are not a constraint. As it was mentioned above, Form 3 3-D printer, that has an X/Y resolution of 25 micrometer and a slightly higher one for Z depending on the chosen layer thicknesses of between 25 and 300 micrometer, has been selected for manufacture as it meets the most demanding features of the CP lens in terms of precision. The tolerances of the Form 3 printer were thoroughly analyzed to adjust the most critical feature sizes of the CP lens: the polarizer slabs dimensions and the lens air holes diameter. The polarizer slabs optimal parameters had to be rigorously adjusted so they exhibited their corresponding optimal value, obtained in Section II-D. Besides, GRIN lens air hole diameter was another critical parameter, as they tended to fill up with excess resin, thus leading to an unsuccessful manufacture. For the diameter of the air holes to be 1 mm in the printed antenna, this value had to be set to 1.15 mm in the layout. Thus, GRIN lens and polarizer are manufactured as a single piece (Fig. 7) by 3-D-SLA technique to experimentally validate some of the simulations previously shown in Section III. To perform the measurements of the proposed design, a standard WR-10 was used to feed the lens antenna by generating an LP spherical wavefront. The performance of the GRIN lens as well as the operation of the polarizer will be evaluated by means of analyzing its capability to convert the impinging spherical LP wave into an

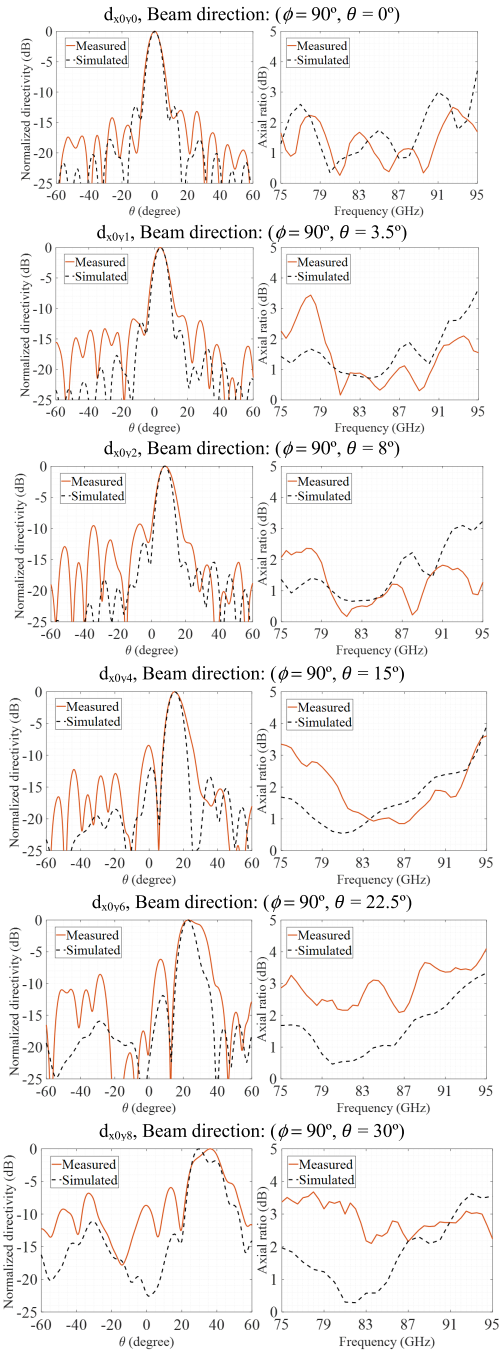

Fig. 8. Measured versus simulated beam reconfigurability (φ = 90°) at 85 GHz and in-band axial ratio at the main lobe angle.

RHCP wave with planar wavefront. The WR-10 will be displaced along y-axis to validate the beam reconfigurability performance. The WR-10, in contrast with the SWG, does barely have any modal coupling, as the TE_{01} does not propagate in the band of interest, which slightly enhances the XP/CP ratio of the design. However, this aspect has been thoroughly analyzed and was not critical to validate the antenna performance.

A dielectric frame was manufactured with the 3-D printer (Fig. 7). It consists of a quadrilateral structure with a 9 × 9 equally 2 mm spaced drilled grid in each corner. Screws are used to fix the position of the dielectric frame, so the lens is located at the optimal focal distance with respect to the WR-10. The focal distance was also experimentally optimized in the measurement setup. Selecting different holes for the screws within the four grids allows the

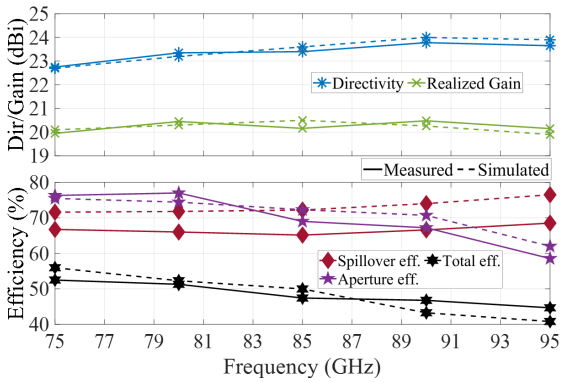

Fig. 9. Measured and simulated directivity, realized gain, total efficiency, aperture efficiency, and spillover efficiency for d_{x0y0} configuration.

displacement of the lens with respect to the feed, thus achieving beam reconfigurability.

Regarding the measurements, in Fig. 8 the measured beam reconfigurability and the in-band axial ratio are evaluated at 85 GHz compared to the simulated results. A remarkable agreement between measured and simulated results is observed for d_{x0y0}, d_{x0y1}, d_{x0y2}, and d_{x0y4} displacements. The d_{x0y6} and d_{x0y8} radiation pattern main lobes slightly widen in comparison to the simulated results, implying a small reduction of directivity. Also, measured in-band axial ratio curves for these two displacements are slightly higher than the simulated results, evidencing the difficulty in the measurement of these two extreme beam steers. As the CP lens is displaced from the WR-10, more surface of the dielectric frame is illuminated, thus altering the expected beam pattern and axial ratio measured results. However, beam reconfiguration capability is demonstrated, as the beam steers from 0° up to 30° as the SWG is displaced along y-axis, as well as the LP to CP conversion capability of the polarizer.

Finally, the main parameters of the design for d_{x0y0} are presented for the whole band in Fig. 9. Directivity maximum values range from 22.75 to 23.78 dBi. Meanwhile, realized gain takes values between 20 and 20.68 dBi. Regarding Gray resin dielectric properties, they were characterized in [26], exhibiting a relative permittivity and loss tangent of 2.73 and 0.016 at 0.2 THz, respectively. However, since Gray resin is not a material designed to be used in RF applications, its dielectric properties may slightly vary from one resin cartridge to another. Thus, it was considered necessary to characterize them again for this work by making use of an optical bench, leading to measured values of $\varepsilon_r = 2.5$ and $\tan\delta = 0.037$. It should be noted that the measured $\tan\delta = 0.037$ loss tangent was considered constant in simulations, despite being a frequency-variable term. This could explain that for some frequencies, measured realized gain takes higher values than simulated realized gain. Besides, the high dielectric losses of the material are an aspect to highlight, as they range from 2.75 to 3.4 dB in the frequency band of the antenna. Dielectric losses in the polarizer as a stand-alone unit have been analyzed, varying between 1.52 dB at 75 GHz and 2.17 dB at 95 GHz. Thus, antenna total radiation efficiency, calculated as the ratio between realized gain and directivity, takes values from 53% at the lowest frequency and 45% at the maximum frequency. Finally, aperture efficiency of the antenna varies from 76.3% at 75 GHz to 58.54% at 95 GHz, whereas spillover efficiency varies from 66.7% at 75 GHz and 68.5% at 95 GHz.

A comparison between the proposed CP lens and other lens antennas found in the literature is shown in Table I. The proposed antenna stands out for its reduced form-factor, and the maximum directivity it achieves with a remarkably high maximum aperture efficiency of 76.3%. Antenna aperture illumination was optimized to achieve the most uniform-like illumination possible. Besides, unlike

TABLE I
COMPARISON BETWEEN LENS ANTENNAS FOUND IN THE STATE-OF-ART

	[8]	[11]	[9]	[7]	This work
Lens type	Hemi spherical	Luneburg	GRIN	FZPL	GRIN
Feed	RWG	RWG	SLA	RWG	SWG
Polarization	Linear	Linear	Linear	Linear	Dual-circular
Freq. (GHz)	290	92.5	28	61.5	85
Dir. (dBi)	31.5	24.3	28.2	35.54*	23.8
Gain (dBi)	30	22.1	21.2	32.7	20.7
Ap. Eff. (%)	38.3*	34.75*	67	59.43*	76.3
BW (%)	30	37.84*	25	11.57	20.8
SLL (dB)	-13	-14	-18	-20	-12
Scan (deg.)	0	$\pm$30	$\pm$58	0	$\pm$30
Volume**	$\varnothing 9.7\lambda_0 \times 10.6\lambda_0$	$\varnothing 8.9\lambda_0 \times 2.5\lambda_0$	$\varnothing 10\lambda_0 \times 7.3\lambda_0$	$\varnothing 24.8\lambda_0 \times 16.8\lambda_0$	$\varnothing 5.7\lambda_0 \times 4.4\lambda_0$

* Not provided. Estimated.
** λ_0 is the free-space wavelength at the central frequency.

the other works, it can generate dual circular polarization from an LP feed. Other works, such as [9], can enhance the scan range of the antenna by means of using a more complex feeding structure, which is usually a higher-cost solution. The present design is an extremely low-budget efficient solution for high-gain dual-circular polarization mm-wave applications where form-factor requirements are a constraint.

V. CONCLUSION

In this communication, a novel design of a dielectric GRIN flat lens with an integrated polarizer to convert dual-LP to dual-CP was presented. An SWG is used to excite vertical (TE_{10}) and horizontal (TE_{01}) polarizations. The polarizer applies a 90° phase shift between the decomposed orthogonal field components of the incident wave, achieving LP to CP conversion. The GRIN lens is used to enhance the radiation in a particular direction, increasing the directivity by generating a plane wave. Thus, the antenna radiates a highly directive RHCP wave when TE_{10} mode is excited in the SWG and a highly directive LHCP wave when the excited mode is the TE_{01}. The main beam can be steered within a demonstrated $\pm$30° scanning range for azimuth and elevation planes, by means of displacing the SWG along the focal plane of the lens. The proposed design was SLA-3-D manufactured as a single piece and measured. All the antenna radiating properties were validated and it has been shown that the utilized material for the CP lens manufacture exhibits non-negligible dielectric losses at this frequency range. Thus, the proposed design serves as a proof of concept and a low loss material for the CP lens manufacture should be used to obtain higher realized gain and total efficiency values. As future lines, the properties of the 3-D-printed polarizer as a stand-alone unit are intended to be assessed, testing its performance with other antennas, such as slot or patch arrays.

REFERENCES

[1] V. W. Paradkar, R. Saha, K. Sreekumar, and S. B. Sharma, "Horn feed with switchable polarization for radar & tracking antenna system," in *Proc. Int. Conf. Range Technol. (ICORT)*, Feb. 2019, pp. 1–3.

[2] D. De and P. K. Sahu, "Design of an endfire microstrip antenna for aircraft collision avoidance system," *IEEE Antennas Wireless Propag. Lett.*, vol. 18, no. 5, pp. 996–1000, May 2019.

[3] T. Zhang, L. Li, H. Xia, X. Ma, and T. J. C. Cui, "A low-cost and high-gain 60-GHz differential phased array antenna in PCB process," *IEEE Trans. Compon., Packag., Manuf. Technol.*, vol. 8, no. 7, pp. 1281–1291, Jul. 2018.

[4] G.-H. Sun and H. Wong, "Millimeter-wave high-gain magneto-electric dipole antenna array with pillbox corporate feed network," *IEEE Trans. Antennas Propag.*, vol. 69, no. 9, pp. 5631–5639, Sep. 2021.

[5] J. M. Monkevich and G. P. Le Sage, "Design and fabrication of a custom-dielectric Fresnel multi-zone plate lens antenna using additive manufacturing techniques," *IEEE Access*, vol. 7, pp. 61452–61460, 2019.

[6] J.-M. Poyanco, F. Pizarro, and E. Rajo-Iglesias, "Cost-effective wideband dielectric planar lens antenna for millimeter wave applications," *Sci. Rep.*, vol. 12, no. 1, p. 4204, Dec. 2022.

[7] M. R. D. Kodnoeih, Y. Letestu, R. Sauleau, E. M. Cruz, and A. Doll, "Compact folded Fresnel zone plate lens antenna for mm-Wave communications," *IEEE Antennas Wireless Propag. Lett.*, vol. 17, no. 5, pp. 873–876, May 2018.

[8] K. Konstantinidis et al., "Low-THz dielectric lens antenna with integrated waveguide feed," *IEEE Trans. THz Sci. Technol.*, vol. 7, no. 5, pp. 572–581, Sep. 2017.

[9] Z. Qu, S.-W. Qu, Z. Zhang, S. Yang, and C. H. Chan, "Wide-angle scanning lens fed by small-scale antenna array for 5G in millimeter-wave band," *IEEE Trans. Antennas Propag.*, vol. 68, no. 5, pp. 3635–3643, May 2020.

[10] S. Manafi, J. M. F. Gonzalez, and D. S. Filipovic, "Design of a perforated flat Luneburg lens antenna array for wideband millimeter-wave applications," in *Proc. 13th Eur. Conf. Antennas Propag.*, Aug. 2019, pp. 1–10.

[11] H. Giddens, A. S. Andy, and Y. Hao, "Multimaterial 3-D printed compressed Luneburg lens for mm-wave beam steering," *IEEE Antennas Wireless Propag. Lett.*, vol. 20, no. 11, pp. 2166–2170, Nov. 2021.

[12] P. Fratilescu, S. Garcia-Ruano, G. Perez-Palomino, and E. Carrasco, "W-band confocal antenna system based on liquid crystal reflectarray for beam scanning applications," in *Proc. 15th Eur. Conf. Antennas Propag. (EuCAP)*, Mar. 2021, pp. 1–5.

[13] M. Letizia, B. Fuchs, A. Skrivervik, and J. R. Mosig, "Circularly polarized homogeneous lens antenna system providing multibeam radiation pattern for HAPS," *URSI Radio Sci. Bull.*, vol. 2010, no. 333, pp. 18–28, Mar. 2010.

[14] Y. Xu and Y.-J. X. Chao Deng, "A feed antenna for dielectric spheres lens in the Ka band," *J. Electr. Electron. Eng. Res.*, vol. 2, no. 5, pp. 122–131, Nov. 2010.

[15] J. Bornemann and V. A. Labay, "Ridge waveguide polarizer with finite and stepped-thickness septum," *IEEE Trans. Microw. Theory Techn.*, vol. 43, no. 8, pp. 1782–1787, Aug. 1995.

[16] Z. Yu and J. Pan, "A novel optimization strategy for the design of large tolerance circular waveguide septum polarizer," in *Proc. IEEE Antennas Propag. Soc. Int. Symp.*, Jun. 2009, pp. 1–4.

[17] D. Martinez-de-Rioja, R. Florencio, J. A. Encinar, E. Carrasco, and R. R. Boix, "Dual-frequency reflectarray cell to provide opposite phase shift in dual circular polarization with application in multibeam satellite antennas," *IEEE Antennas Wireless Propag. Lett.*, vol. 18, no. 8, pp. 1591–1595, Aug. 2019.

[18] X. Li, J. Xiao, and J. Yu, "Long-distance wireless mm-Wave signal delivery at W-band," *J. Lightw. Technol.*, vol. 34, no. 2, pp. 661–668, Jan. 15, 2016.

[19] A. Sabharwal, P. Schniter, D. Guo, D. W. Bliss, S. Rangarajan, and R. Wichman, "In-band full-duplex wireless: Challenges and opportunities," *IEEE J. Sel. Areas Commun.*, vol. 32, no. 9, pp. 1637–1652, Sep. 2014.

[20] K. X. Wang and H. Wong, "A wideband millimeter-wave circularly polarized antenna with 3-D printed polarizer," *IEEE Trans. Antennas Propag.*, vol. 65, no. 3, pp. 1038–1046, Mar. 2017.

[21] T. Mcmanus, R. Mittra, and C. Pelletti, "A comparative study of flat and profiled lenses," in *Proc. IEEE Int. Symp. Antennas Propag.*, Jul. 2012, pp. 1–2.

[22] A. Petosa and A. Ittipiboon, "Design and performance of a perforated dielectric Fresnel lens," *IEE Proc. Microw., Antennas Propag.*, vol. 150, no. 5, pp. 309–314, Oct. 2003.

[23] H. Quan, T. Zhang, H. Xu, S. Luo, J. Nie, and X. Zhu, "Photo-curing 3D printing technique and its challenges," *Bioactive Mater.*, vol. 5, no. 1, pp. 110–115, May 2020.

[24] T. Finnes, "High-definition 3D printing—Comparing SLA and FDM printing technologies," *J. Undergrad. Res.*, vol. 13, pp. 167–178, Dec. 2015.

[25] J. M. Felicio, C. A. Fernandes, and J. R. Costa, "Complex permittivity and anisotropy measurement of 3D-printed PLA at microwaves and millimeter-waves," in *Proc. 22nd Int. Conf. Appl. Electromagn. Commun. (ICECOM)*, Sep. 2016, pp. 1–6.

[26] N. Duangrit, B. Hong, A. D. Burnett, P. Akkaraekthalin, I. D. Robertson, and N. Somjit, "Terahertz dielectric property characterization of photopolymers for additive manufacturing," *IEEE Access*, vol. 7, pp. 12339–12347, 2019.